Trade-offs in Size and Performance for a Point Source Interferometer Gyroscope

Gregory W. Hoth, Bruno Pelle, John Kitching, and Elizabeth A. Donley
NIST, Boulder, CO 80305. gregory.hoth@nist.gov

***Abstract*—Point source interferometry (PSI) is a promising technique that could lead to a compact, high-performance gyroscope based on atom interferometry. We consider the trade-offs in size and performance with PSI. In particular, we discuss the sensitivity and dynamic range for a simple PSI gyroscope with an evacuated volume ranging from 1 mm^3 to 10 cm^3. We also discuss the stability required for the initial atomic distribution in order to achieve part-per-million scale factor stability.**

I. Introduction

Light pulse atom interferometers (LPAIs) are an emerging technology for precision inertial sensors [1]–[3]. LPAIs have demonstrated sensitivities to accelerations of 4.2×10^{-8} m/s$^2\sqrt{\text{Hz}}$ [4] and rotations of 80 $\mu\text{deg}/\sqrt{\text{hr}}$ [5]. However, the systems that have achieved this level of performance are delicate, laboratory instruments with a characteristic size of meters. To enable the use of these sensors in applications such as gravimetric surveys and inertial navigation, it is desirable to reduce the size and complexity of LPAIs. Recently, a new detection strategy known as point source interferometry (PSI) has been introduced [6] which has the potential to enable a navigation-grade LPAI gyroscope with an evacuated volume of approximately 1 cm^3.

Here we discuss the rotation sensitivity and dynamic range that could be achieved with a PSI gyroscope with an emphasis on the trade-offs between sensor size and performance. Section II reviews the physics of the PSI measurement. Section III estimates the sensitivity of the PSI scheme and quantifies the size-sensitivity trade-offs for a simple PSI gyroscope. Section IV considers two limits to the dynamic range of the PSI measurement. Section V discusses the stability required for the initial distribution. Finally, section VI concludes the paper.

II. PSI measurement scheme

In LPAIs, laser pulses are used to coherently manipulate atomic wave packets. An interferometer is realized by arranging for the wave packets to split and then recombine after traveling over two or more distinct paths. If the paths enclose an area, the interferometer will be sensitive to rotations due to the matter-wave analog of the Sagnac effect [1]. Many variations on this idea have been studied over the years, but the most common approach has been to use stimulated Raman transitions to produce atomic trajectories analogous to a Mach-Zehnder optical interferometer [7]. This requires a sequence of three pulses, which is shown schematically in Fig. 1.

The interferometer pulse sequence begins at the the left in Fig. 1 with an atom in an internal state $|0\rangle$ and momentum $\vec{p} = mv\hat{x}$. First, an initial beamsplitter or $\pi/2$ pulse is applied. This pulse puts each atom into a coherent superposition of two

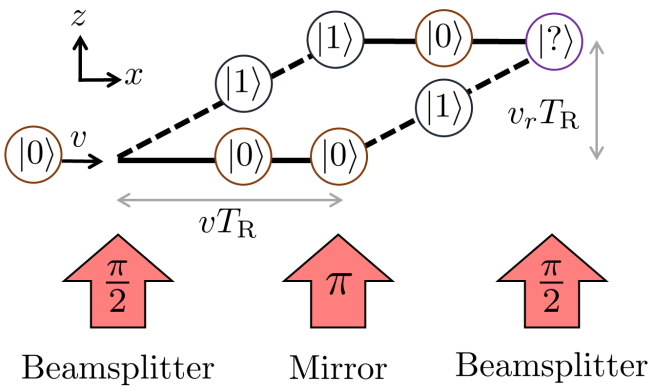

Fig. 1. A schematic diagram of the Mach-Zehnder LPAI pulse sequence used in the PSI gyroscope. An atom with two internal states $|0\rangle$ and $|1\rangle$ is traveling to the right. Through its interaction with the light pulses, the atom is split into a coherent superposition of two states and then recombined. The lines indicate the classical trajectories followed by the components of the atomic wave packet. The area enclosed by the two trajectories is proportional to the velocity transferred to the atom by the laser pulses, which is given by $v_r = \hbar k_{\text{eff}}/m$. The atom's final state depends on the difference between the phase accumulated on the two paths.

states, $|0, \vec{p}\rangle$ and $|1, \vec{p} + \hbar\vec{k}_{\text{eff}}\rangle$. Crucially, the momentum of the $|1\rangle$ component of the superposition is increased by $\hbar\vec{k}_{\text{eff}}$, where $\vec{k}_{\text{eff}}$ is the effective wave-vector for the Raman transitions. This momentum kick results from an atom absorbing and emitting photons during its interaction with the light pulse. After the first pulse, the atoms propagate freely for a period T_{R}, which allows the two components of the superposition to separate. Then, a mirror or π pulse is applied which exchanges the two parts of the superposition. After a second free evolution period, the two components of the superposition overlap, and a final $\pi/2$ pulse recombines them. The state of the atoms after the pulse sequence is determined by the relative phase shift between the two paths [8]. The probability for an atom to be detected with internal state $|1\rangle$ can be described as

$$p = \frac{1}{2}\left(1 + c\sin(\Phi)\right), \tag{1}$$

where c is the contrast and Φ is the phase. Due to the Sagnac effect, a rotation of the interferometer produces a phase shift

$$\Phi_\Omega = \frac{2m}{\hbar}\vec{\Omega}\cdot\vec{A} = 2\vec{k}_{\text{eff}}\cdot\left(\vec{\Omega}\times\vec{v}\right)T_{\text{R}}^2, \tag{2}$$

where $\vec{A} = \left(\hbar\vec{k}_{\text{eff}}/m\right)T_{\text{R}} \times (\vec{v}\,T_{\text{R}})$ is the area enclosed by the interferometer and $\vec{\Omega}$ is the rotation rate.

In order to realize a gyroscope with this three-pulse sequence, we need to separate Φ_Ω from other phase shifts. In par-

ticular, accelerations of the interferometer also produce phase shifts which are given by $\Phi_a = \vec{k}_{\rm eff} \cdot \vec{a}\, T_{\rm R}^2$. Φ_Ω and Φ_a can be distinguished by exploiting the velocity dependence of Φ_Ω. This has typically been accomplished by implementing two simultaneous atom interferometers with counter-propagating atomic beams [5], [9] or launched clouds of cold atoms [10]–[12]. This strategy has led to excellent performance, but it also increases the size and complexity of the apparatus.

In PSI, counter-propagating atoms are obtained with a single atomic source by exploiting the residual velocity distribution of a cloud of cold atoms. The key idea is that the expansion of the cloud during the interferometer pulse sequence leads to a correlation between each atom's final position, $\vec{r}$, and its initial velocity, $\vec{v}$. If the initial cloud is infinitesimally small, the correlation is perfect, and we have $\vec{r} = 2T_{\rm R}\vec{v}$. In this point-source limit, Eq. 2 becomes

$$\Phi_\Omega = \left(\vec{k}_{\rm eff} \times \vec{\Omega} T_{\rm R}\right) \cdot \vec{r} = \vec{k}_\Omega \cdot \vec{r}, \tag{3}$$

where $\vec{k}_\Omega$ describes a spatial gradient in the interferometer phase. This phase gradient will produce a spatial fringe pattern in the state of the atoms, which can be detected by imaging the cloud. The two components of the rotation vector orthogonal to $\vec{k}_{\rm eff}$ can be determined from the magnitude and orientation of the phase gradient.

Although it is not possible to achieve an infinitesimally small initial cloud, these spatial fringe patterns are surprisingly robust. They can be detected even if the cloud expands by less than a factor of two during the interferometer sequence [13]. With a finite initial cloud size, the correlation between the atoms' initial velocities and their final positions will be blurred because atoms from different regions of the initial cloud will arrive at the same final position with different velocities. This blurring leads to a loss of fringe contrast and a shift in the detected phase gradient which can limit the dynamic range and stability of a PSI gyroscope [13]. These effects are considered in more detail below.

With PSI, it is not necessary to use multiple atomic sources or launch the cold atom cloud. This suggests that a PSI gyroscope could be simpler and more compact than other LPAI gyroscopes. PSI also has an advantage in the trade-off between size and sensitivity compared to systems based on thermal beams or launched cold atom clouds because of the low velocity of the laser-cooled atoms. This can be seen by noting the interferometer period is limited to $T_{\rm R} = L/2v$, where L is the length of the interrogation region. Thus, the scale factor connecting the phase shift to the rotation rate can be written $F = k_{\rm eff} L^2/2v$. For a fixed L, the rotation scale factor can be increased by decreasing the atomic velocity. A characteristic velocity for laser-cooled atoms is $v \sim 0.1$ m/s compared to $v \sim 300$ m/s for thermal atomic beams [5], [9] and $v \sim 5$ m/s for launched cold atom clouds [10]–[12].

The interferometer period is also constrained by the atoms' acceleration due to gravity. In this case, there is a velocity $v_{\rm opt} = L/2T_{\rm R}$ which optimizes the rotation scale-factor. If the atoms are allowed to fall a distance L in a time $2T_{\rm R}$, then $v_{\rm opt} = \sqrt{Lg/2}$. With $L = 1$ cm, we have $v_{\rm opt} \approx 0.2$ m/s, which is similar to the velocities naturally achieved with laser cooling. This suggests PSI is well suited to realizing an LPAI gyroscope with an interrogation volume on the order of $1\ {\rm cm}^3$.

III. Sensitivity

In order to measure rotations with PSI, we must determine the phase gradient k_Ω from a spatially resolved measurement of the transition probability. The minimum phase gradient that can be detected in a single shot, $k_{\Omega,\min}$, can be estimated by considering an initial cloud with N atoms divided equally between two velocities, $v_\pm = \pm L/4T_{\rm R}$, where L is the size of the detection region. From Eq. 1, the phase gradient is given by $k_\Omega = 2\left(p_+ - p_-\right)/Lc$, where $p_\pm$ is the probability of detecting the atoms with velocity $v_\pm$ in state $|1\rangle$. Then, we have $k_{\Omega,\min} = 2\sqrt{2}\sigma_p/Lc$, where σ_p is the uncertainty in the measurement of $p_\pm$. The uncertainty will be limited by quantum projection noise [14], which corresponds to $\sigma_p = \sqrt{1/2N}$ since there are $N/2$ atoms with each velocity. Putting it all together, we find $k_{\Omega,\min} = 2/Lc\sqrt{N}$ for this model.

In a real system, the initial cloud will have a continuous distribution of velocities, and the atoms will be spread throughout the detection region. If the final cloud is modeled as a uniform density distribution, we find that $k_{\Omega,\min}$ is increased by a factor of $\sqrt{3}$ from the simple model considered above [15]. After converting $k_{\Omega,\min}$ to a rotation rate with Eq. 3 and accounting for the repetition rate of the sensor, we find that the PSI rotation sensitivity is given by

$$\delta\Omega = \frac{\sqrt{12}}{k_{\rm eff}\, L\, T_{\rm R}} \frac{\sqrt{T_{\rm c}}}{\rm SNR}, \tag{4}$$

where L is the length of the region used to estimate the phase gradient, $T_{\rm c}$ is the cycle period, and SNR is the signal-to-noise ratio. For quantum projection noise limited detection, ${\rm SNR} = c\sqrt{N}$.

The sensitivity can be optimized by maximizing the SNR, $T_{\rm R}$, and the size of the detection region while minimizing $T_{\rm c}$. There are several trade-offs in size and sensitivity. First, the size of the device clearly limits L. The device size also limits T_R because the atoms must not escape from the interrogation region due to their initial velocity or their acceleration due to gravity. Finally, there is a trade-off between size and SNR because the number of cold atoms available for use in the measurement scales strongly with the size of the device [16].

In order to explore the performance that could be achieved with a PSI gyroscope, it is useful to analyze a simple model system. We consider a cubic volume with side length L, which is used to prepare, interrogate, and detect the atoms. Cold atoms can be produced by use of a vapor-cell Magneto-Optical Trap (MOT) with trapping beams that also have a diameter L [17]. For diameters $L > 2$ mm, the atom number is expected to scale as $L^{3.6}$ [16], [18], [19], which means the SNR will scale as $L^{1.8}$. The interferometer period will be limited by the atoms' free fall. We choose $T_{\rm R} = \sqrt{L/4g}$ so that the cloud falls a distance $L/2$ during the pulse sequence. To ensure the detection region is not limited by the size of the final cloud, the cloud temperature, T, must be set so that the cloud expands to fill the available space. The expanded cloud can be approximated as a Gaussian density distribution with a $1/e^2$ diameter given by $8T_{\rm R}\sqrt{k_B T/m}$. We set $T = mgL/16k_B$ so that this $1/e^2$ diameter is equal to L. With this choice, approximately 90% of the atoms in the expanded cloud are contained in the detection region. Since the expanded cloud largely overlaps with the MOT capture

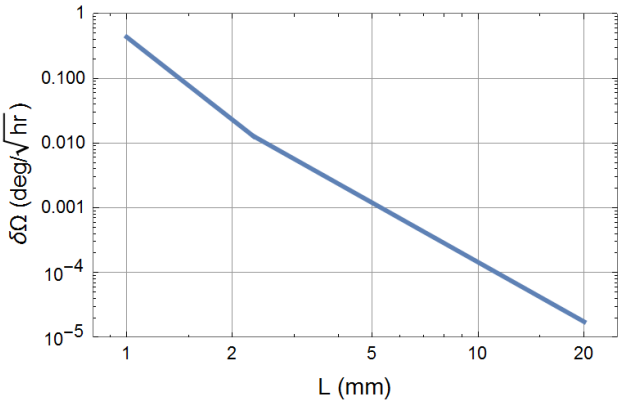

Fig. 2. Rotation sensitivity vs size of interrogation region for our model PSI gyroscope with ^{87}Rb atoms. $\delta\Omega$ was estimated with Eq. 4 assuming quantum projection noise limited SNR. The MOT atom numbers, N, were estimated with the data from [19]. With perfect recapture and $T_c = 4T_R$, N is reduced by a factor of 2 since the MOT is on during half of the cycle [12]. The kink in the curve near $L = 2$ mm comes about because N scales as L^6 for MOTs with small trapping regions [21].

TABLE I. SENSITIVITY AND PARAMETERS VS SIZE OF INTERROGATION REGION FOR THE MODEL PSI GYROSCOPE.

L (mm)	T_R (ms)	T (μK)	N	$\delta\Omega$ (deg/$\sqrt{\text{hr}}$)
1	5.1	6.4	2.3×10^3	4.4×10^{-1}
2	7.1	13	1.5×10^5	2.3×10^{-2}
5	11	32	5.4×10^6	1.2×10^{-3}
10	16	64	6.6×10^7	1.4×10^{-4}
20	23	130	8×10^8	1.7×10^{-5}

region, it will be possible to recapture the cold atoms from run to run, enabling short cycle periods. For this example, we set the cycle period as $T_c = 4T_R$. Previous work on high data-rate atom interferometers suggests this choice leaves sufficient time for experimental details like initial state preparation and atom recapture [12], [20].

The estimated sensitivity for this model system is shown as a function of L in Fig. 2. The model parameters for several different values of L are summarized in Table I. This calculation indicates a PSI gyroscope with an evacuated volume with a characteristic size L in the range 5-10 mm could achieve sensitivity that is interesting for navigation applications. One can also imagine ways to improve the sensitivity such as launching the atom cloud to increase T_R. It is also important to consider the laser performance required to achieve high contrast interferometer signals with quantum projection noise limited SNR, but we leave this question for future work.

IV. DYNAMIC RANGE

There are two effects that constrain the maximum rotation rate that could be detected with PSI. The first effect is due to the finite size of the atomic wave packets. When $\Omega \neq 0$, the two interferometer arms shown in Fig. 1 do not overlap at the end of the pulse sequence because the rotation changes the direction of the momentum kick delivered by the mirror pulse [22]. The displacement between the two interferometer arms at the end of the sequence is given by $\epsilon = 2\hbar k_{\text{eff}} \Omega T_R^2/m$. When this displacement is comparable to the wave packet size λ, the interferometer contrast will be significantly reduced. This

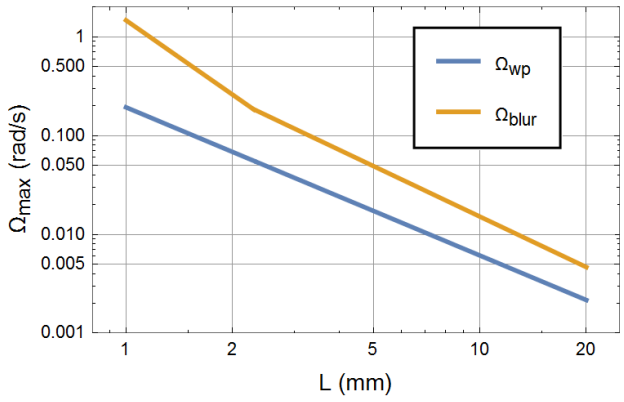

Fig. 3. Limiting rotation rates vs size of interrogation region for the model PSI gyroscope with ^{87}Rb atoms. The wave packet size was estimated as $\lambda = h/mv_{\text{avg}}$ where $v_{\text{avg}} = \sqrt{(8/\pi)\, k_B T/m}$ is the average speed for the thermal distribution.

leads to a maximum rotation rate of

$$\Omega_{\text{wp}} = \frac{m\lambda}{2\hbar k_{\text{eff}}} \frac{1}{T_R^2}. \quad (5)$$

The wave packet size λ can be estimated from the de Broglie relation $\lambda = h/p$.

The second effect that limits the dynamic range is due to the finite size of the initial cloud. The blurring of the correlation between position and velocity can be quantified by modeling the initial cloud as a sphere with diameter d. In this case, the range of velocities that arrive at the same final position in the expanded cloud is given by $\delta v = d/2T_R$. Via Eq. 2, this corresponds to a range of phase shifts which must be averaged over. When this range of phase shifts reaches 2π, the fringe contrast will wash out. This leads to a maximum rotation rate of

$$\Omega_{\text{blur}} = \frac{2\pi}{k_{\text{eff}} d} \frac{1}{T_R}. \quad (6)$$

The initial cloud size obtained with a MOT can be estimated by modeling the cloud as a uniform sphere with density n_m. For a wide range of atom numbers, the cloud density is limited to $n_m \approx 3 \times 10^{10}$ atoms/cm^3 by photon rescattering [18], [23].

Figure 3 shows these two limits to the dynamic range as a function of L for the model PSI gyroscope introduced in Sec. III. We find that Ω_{wp} and Ω_{blur} are expected to have the same order of magnitude in this case.

V. STABILITY AND THE INITIAL ATOMIC DISTRIBUTION

Although the PSI scheme offers several advantages compared to other LPAI gyroscopes, these benefits come with a cost. The PSI fringe patterns depend on the details of the initial atomic distribution, and this can lead to frequency shifts and non-linearities in the relationship between the detected fringe pattern and the rotation rate [15]. This means it will be important to stabilize the initial atomic distribution. The required level of stabilization can be estimated by modeling the initial cloud as a Gaussian density distribution. In this case, it is possible to derive an exact expression for the detected PSI fringes [13]. We find that the initial distribution leads to a shift in the gyroscope scale factor, which can be expressed as

$$F_g = F_{ps} \left(1 - \sigma_0^2/\sigma_f^2\right), \quad (7)$$

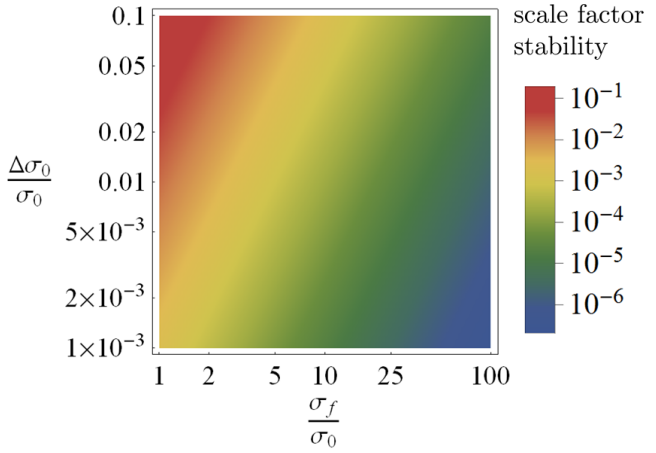

Fig. 4. Scale factor fluctuations (color) as a function of the expansion ratio and the fluctuations in the initial cloud size. The cloud temperature is assumed to be completely stable.

where σ_0 and σ_f characterize the width of the initial cloud and the expanded cloud, and F_ps is the scale factor in the point-source limit. From Eq. 3, we have $F_\mathrm{ps} = k_\mathrm{eff} T_\mathrm{R}$. From Eq. 7, we can calculate the effect of fluctuations in the initial size and temperature on the scale factor. The result is

$$\frac{\Delta F}{F} = \frac{\sigma_0^2}{\sigma_\mathrm{f}^2}\sqrt{\left(2\frac{\Delta\sigma_0}{\sigma_0}\right)^2 + \left(\frac{\Delta T}{T}\right)^2}, \tag{8}$$

where Δy represents the fluctuations in the quantity y. Figure 4 shows the expected fluctuations in the scale factor as a function of the fluctuations in the initial cloud size and the expansion ratio $\sigma_\mathrm{f}/\sigma_0$. For navigation applications, it is desirable to have a scale factor stability on the order of 10^{-6}. This level of stability could be achieved with an expansion factor of 25 and fluctuations in the initial cloud size of 10^{-3}. This might be achieved by using an optical dipole trap to compress and stabilize the initial atomic distribution [17]. In this case, the trapping potential is approximately quadratic and the initial cloud would have a Gaussian density distribution.

VI. Conclusion

There is a wide design space to explore for a compact LPAI gyroscope based on PSI. We hope these estimates of the sensitivity, dynamic range, and stability requirements will be useful tools in the on-going work to investigate and optimize the PSI technique. A promising direction for future work is to consider PSI in micro-gravity. In this environment, the low velocity of laser-cooled atoms would lead to long interrogation periods and high sensitivity with a compact device.

Acknowledgment

This work was funded by NIST, a US government agency, and it is not subject to copyright.

References

[1] A. D. Cronin, J. Schmiedmayer, and D. E. Pritchard, "Optics and interferometry with atoms and molecules," *Reviews of Modern Physics*, vol. 81, no. 3, pp. 1051–1129, Jul. 2009.

[2] J. Kitching, S. Knappe, and E. Donley, "Atomic Sensors—A Review," *IEEE Sensors Journal*, vol. 11, no. 9, pp. 1749 –1758, Sep. 2011.

[3] B. Barrett, A. Bertoldi, and P. Bouyer, "Inertial quantum sensors using light and matter," *Physica Scripta*, vol. 91, no. 5, p. 053006, 2016.

[4] Z.-K. Hu, B.-L. Sun, X.-C. Duan, M.-K. Zhou, L.-L. Chen, S. Zhan, Q.-Z. Zhang, and J. Luo, "Demonstration of an ultrahigh-sensitivity atom-interferometry absolute gravimeter," *Physical Review A*, vol. 88, no. 4, p. 043610, Oct. 2013.

[5] D. S. Durfee, Y. K. Shaham, and M. A. Kasevich, "Long-Term Stability of an Area-Reversible Atom-Interferometer Sagnac Gyroscope," *Physical Review Letters*, vol. 97, no. 24, p. 240801, Dec. 2006.

[6] S. M. Dickerson, J. M. Hogan, A. Sugarbaker, D. M. S. Johnson, and M. A. Kasevich, "Multiaxis Inertial Sensing with Long-Time Point Source Atom Interferometry," *Physical Review Letters*, vol. 111, no. 8, p. 083001, Aug. 2013.

[7] M. Kasevich and S. Chu, "Atomic interferometry using stimulated Raman transitions," *Physical Review Letters*, vol. 67, no. 2, pp. 181–184, Jul. 1991.

[8] C. J. Bordé, "Atomic interferometry with internal state labelling," *Physics Letters A*, vol. 140, no. 1, pp. 10–12, Sep. 1989.

[9] T. L. Gustavson, A. Landragin, and M. A. Kasevich, "Rotation sensing with a dual atom-interferometer Sagnac gyroscope," *Classical and Quantum Gravity*, vol. 17, pp. 2385–2398, Jun. 2000.

[10] B. Barrett, R. Geiger, I. Dutta, M. Meunier, B. Canuel, A. Gauguet, P. Bouyer, and A. Landragin, "The Sagnac effect: 20 years of development in matter-wave interferometry," *Comptes Rendus Physique*, vol. 15, no. 10, pp. 875–883, Dec. 2014.

[11] G. Tackmann, P. Berg, S. Abend, C. Schubert, W. Ertmer, and E. M. Rasel, "Large-area Sagnac atom interferometer with robust phase read out," *Comptes Rendus Physique*, vol. 15, pp. 884–897, Dec. 2014.

[12] A. V. Rakholia, H. J. McGuinness, and G. W. Biedermann, "Dual-Axis High-Data-Rate Atom Interferometer via Cold Ensemble Exchange," *Physical Review Applied*, vol. 2, no. 5, p. 054012, Nov. 2014.

[13] G. W. Hoth, B. Pelle, S. Riedl, J. Kitching, and E. A. Donley, "Point source atom interferometry with a cloud of finite size," *Applied Physics Letters*, vol. 109, no. 7, p. 071113, Aug. 2016.

[14] W. M. Itano, J. C. Bergquist, J. J. Bollinger, J. M. Gilligan, D. J. Heinzen, F. L. Moore, M. G. Raizen, and D. J. Wineland, "Quantum projection noise: Population fluctuations in two-level systems," *Physical Review A*, vol. 47, no. 5, pp. 3554–3570, May 1993.

[15] G. W. Hoth, "Development and characterization of an interferometer based on an expanding ball of atoms," Ph.D. dissertation, University of Colorado, Boulder, 2016.

[16] K. Lindquist, M. Stephens, and C. Wieman, "Experimental and theoretical study of the vapor-cell Zeeman optical trap," *Physical Review A*, vol. 46, no. 7, pp. 4082–4090, Oct. 1992.

[17] H. J. Metcalf and P. van der Straten, *Laser Cooling and Trapping*. New York, NY: Springer New York, 1999.

[18] K. E. Gibble, S. Kasapi, and S. Chu, "Improved magneto-optic trapping in a vapor cell," *Optics Letters*, vol. 17, no. 7, pp. 526–528, Apr. 1992.

[19] G. W. Hoth, E. A. Donley, and J. Kitching, "Atom number in magneto-optic traps with millimeter scale laser beams," *Optics Letters*, vol. 38, no. 5, p. 661, Mar. 2013.

[20] H. J. McGuinness, A. V. Rakholia, and G. W. Biedermann, "High data-rate atom interferometer for measuring acceleration," *Applied Physics Letters*, vol. 100, no. 1, pp. 011 106–011 106–4, Jan. 2012.

[21] S. Pollock, J. P. Cotter, A. Laliotis, F. Ramirez-Martinez, and E. A. Hinds, "Characteristics of integrated magneto-optical traps for atom chips," *New Journal of Physics*, vol. 13, no. 4, p. 043029, Apr. 2011.

[22] S.-Y. Lan, P.-C. Kuan, B. Estey, P. Haslinger, and H. Müller, "Influence of the Coriolis Force in Atom Interferometry," *Physical Review Letters*, vol. 108, no. 9, p. 090402, Feb. 2012.

[23] C. G. Townsend, N. H. Edwards, C. J. Cooper, K. P. Zetie, C. J. Foot, A. M. Steane, P. Szriftgiser, H. Perrin, and J. Dalibard, "Phase-space density in the magneto-optical trap," *Physical Review A*, vol. 52, no. 2, pp. 1423–1440, Aug. 1995.